

Neutral-atom entanglement using adiabatic Rydberg dressing

Anupam Mitra,^{1,2,*} Sivaprasad Omanakuttan^{1,2,†} , Michael J. Martin,^{3,1,‡} Grant W. Biedermann,^{4,§} and Ivan H. Deutsch^{1,2,||} 

¹Center for Quantum Information and Control, University of New Mexico, Albuquerque, New Mexico 87131, USA

²Department of Physics and Astronomy, University of New Mexico, Albuquerque, New Mexico 87106, USA

³Los Alamos National Laboratory, Los Alamos, New Mexico 87545, USA

⁴Department of Physics and Astronomy, University of Oklahoma, Norman, Oklahoma 73019, USA



(Received 1 September 2022; accepted 16 February 2023; published 15 June 2023)

We revisit the implementation of a two-qubit entangling gate, the Mølmer-Sørensen gate, using the adiabatic Rydberg dressing paradigm for neutral atoms as studied in [A. Mitra *et al.*, *Phys. Rev. A* **101**, 030301(R) (2020)]. We study the implementation of rapid adiabatic passage using a two-photon transition, which does not require the use of an ultraviolet laser, and can be implemented using only amplitude modulation of one field with all laser frequencies fixed. We find that entangling gate fidelities, comparable to the one-photon excitation, are achievable with the two-photon excitation. Moreover, we address how the adiabatic dressing protocol can be used to implement entangling gates outside the regime of a perfect Rydberg blockade. We show that, by using adiabatic dressing, we can achieve scaling of the gate fidelity set by the fundamental limits to entanglement generated by the Rydberg interactions while simultaneously retaining a limited population in the doubly excited Rydberg state. This allows for fast high-fidelity gates for atoms separated beyond the blockade radius.

DOI: [10.1103/PhysRevA.107.062609](https://doi.org/10.1103/PhysRevA.107.062609)

I. INTRODUCTION

Optically trapped arrays of neutral atoms with tunable electric dipole-dipole interactions (EDDI) are a promising platform for scalable quantum computation [1–13], quantum simulations [14–26], and quantum metrology [27–29]. A variety of protocols have been studied to create entanglement between atomic qubits using the strong EDDI of Rydberg atoms [5,30–37], and have been demonstrated in alkali atoms including cesium and rubidium [2,5,10,11,16,38–43] and in alkaline earth atoms including strontium and ytterbium [29,44,45]. Given rapid advances in the field, we seek to revisit some practical considerations and fundamental limits for qubit entanglement that are achievable with adiabatic Rydberg dressing of ground state atoms.

In particular, we consider the use of adiabatic Rydberg dressing [29,32,37,43,46], a powerful tool for robustly creating entanglement in atomic-clock qubits. In this approach, the Rydberg character is adiabatically admixed into one of the clock states through a chirp of the laser frequency and/or intensity ramp [29,37,43]. The resulting light shift of the dressed state is then mediated by the Rydberg EDDI, leading to entanglement [29,37,43]. This tool was implemented to create Bell states of clock qubits in the microwave [47] and optical regimes [29] and for studies of many-body physics [14,15,17]. Schemes for implementing two-qubit entangling quantum logic gates based on adiabatic Rydberg dressing

were studied theoretically [32,34,36,37] and recently demonstrated [29,43].

Adiabatic Rydberg dressing is most naturally implemented using a one-photon transition between a clock state and a high-lying Rydberg state [14,15,17,32,37,47]. Such an approach requires a high-power ultraviolet laser, which is technically challenging and can lead to adverse effects, such as photoelectric charging of dielectrics and spurious electric fields. Adiabatic Rydberg dressing would be more simply be achieved through a standard two-photon transition that is typically used for Rydberg excitation, but this may lead to other challenges due to additional decoherence and spurious light shifts from off-resonant excitation to the intermediate state [48,49]. We revisit this problem here and show that a two-photon excitation is well matched to adiabatic Rydberg dressing, with additional light shifts facilitating adiabatic passages by modulating only one laser amplitude. With the current state of the art, decoherence will not greatly reduce gate fidelity. Moreover, dominant inhomogeneities can be removed in this protocol through spin echoes, as studied in Ref. [37] implemented in Refs. [29,43].

Beyond the practical consideration of two-photon excitation for adiabatic Rydberg dressing, we revisit the limits of gate fidelity from a finite Rydberg-state lifetime and finite interaction energy between Rydberg states that can be generated using adiabatic Rydberg dressing of ground-state atoms. While the basic entangling interaction is due to the interactions between Rydberg states with strength $|V|$, in protocols that employ the Rydberg blockade, the speed of the gate is limited by the effective Rabi frequency of the coupling laser Ω_{eff} , as in the seminal work of the authors of Ref. [30]. Rydberg dressing under a strong blockade, where the admixture of the doubly excited Rydberg states is small and often negligible requires $\hbar\Omega_{\text{eff}} \ll |V|$. As such, one cannot

*anupam@unm.edu

†somanakuttan@unm.edu

‡mmartin@lanl.gov

§biedermann@ou.edu

||ideutsch@unm.edu

achieve the fundamental scaling in the gate error rate set by the ratio $2\pi\hbar\Gamma/|V|$ for a characteristic decoherence rate Γ [4]. Adiabatic Rydberg dressing has generally also operated in the strong blockade regime [29,32,37,43,50], but this is not essential to the protocol. In principle, adiabatic admixtures that include doubly excited Rydberg levels will strongly increase the entangling energy or may be used to maintain atoms separated beyond the blockade radius where they can be more easily individually addressed, yet still achieve fast gates. Rydberg-mediated entanglement beyond the strong blockade regime was demonstrated using finely tuned two-atom Rabi oscillations [42]. In addition, some quantum simulation schemes implementing interacting spin models did not assume strong blockade in a multiatom array, allowing the implementation of elaborate interaction graphs between atoms in one-dimensional [16,20,21] and two-dimensional geometries [10–12,22,23,49].

We show here that, by going beyond the perfect blockade regime, one can use adiabatic Rydberg dressing to reach the fundamental scaling of entangling gate fidelity [51]. Such an approach may become more feasible, e.g., by using bound states of doubly excited Rydberg macrodimers [52] that have been well resolved [52,53] and can be employed for such coherent control of entanglement [53]. In addition, we find that one can implement entangling gates in the weak blockade regime using an adiabatic Rydberg dressing scheme that requires only a limited population in the doubly excited Rydberg state, similar to that found in Ref. [42] and unlike some other protocols for entangling gates [3–5,40]. Thus, protocols that extend beyond the perfect blockade regime may enable even more powerful schemes for neutral atom quantum information processing.

The remainder of this article is organized as follows. In Sec. II we discuss the implementation of two-photon adiabatic Rydberg dressing passages for creating high-fidelity entangling gates. We show that fidelities $\mathcal{F} > 0.99$ are possible with state-of-the-art experiments. In Sec. III we study the scaling of the Rydberg-dressing entangling energy in the regimes of strong and weak blockades and show that we can reach the fundamental scaling as predicted in Ref. [51] when we allow a small admixture of doubly excited Rydberg states during adiabatic Rydberg dressing. In Sec. IV we conclude and give an outlook toward future applications.

II. ENTANGLING GATES WITH ADIABATIC DRESSING

We study the implementation of two-qubit gates with qubits encoded in clock states, e.g., $|0\rangle \equiv |(ns), {}^2S_{1/2}, F, m=0\rangle$, $|1\rangle \equiv |(ns), {}^2S_{1/2}, F', m=0\rangle$ for alkali atoms and $|0\rangle \equiv |(ns)^2, {}^1S_0\rangle$, $|1\rangle \equiv |(nsnp), {}^3P_0\rangle$ for alkaline earth-like atoms. Entanglement is generated by the adiabatic dressing of the $|1\rangle$ -state through a one- or two-photon transition to an excited Rydberg state $|r\rangle$ with high principle quantum number n_r . For a one-photon ultraviolet transition, $|r\rangle \equiv |(n_r p), {}^2P_J\rangle$ for alkalis and $|r\rangle \equiv |(nsn_r s), {}^3S_1\rangle$ for alkaline earths. In the two-photon case, $|r\rangle \equiv |(n_r s), {}^2S_{1/2}\rangle$ for alkalis and $|r\rangle \equiv |(nsn_r p), {}^3P_J\rangle$ for alkaline earths, with an intermediate auxiliary state $|a\rangle \equiv |(n_a p), {}^2P_J\rangle$ or $|a\rangle \equiv |(nsn_a s), {}^3S_1\rangle$, respectively. The generation of entanglement is fundamentally limited by decoherence due to the lifetime of $|r\rangle$ and $|a\rangle$,

which depend on the choice of principal quantum numbers n_r and n_a . The schematics for one- and two-photon coupling are shown in Figs. 1(a) and 1(b), respectively.

We consider two atoms symmetrically coupled by uniform laser fields. As only the $|1\rangle$ state is coupled to $|r\rangle$ (in a one- or two-photon transition), the Hamiltonian takes the form

$$\hat{H} = \hat{H}_1 \otimes |0\rangle\langle 0| + |0\rangle\langle 0| \otimes \hat{H}_1 + \hat{H}_{1,1}, \quad (1)$$

where \hat{H}_1 is the Hamiltonian for one atom in $|1\rangle$ coupled to $|r\rangle$ and $\hat{H}_{1,1}$ is the two-atom coupling, including the Rydberg-mediated EDDI. We define the Rabi frequencies $\Omega_{\alpha\beta}$ and detunings $\Delta_{\alpha\beta}$ for each of the corresponding $|\alpha\rangle \leftrightarrow |\beta\rangle$ transitions as shown in Figs. 1(a) and 1(b). For a two-photon excitation, we consider the regime $\Omega_{1a} \ll |\Delta_{1a}|$ so that the intermediate state can be adiabatically eliminated. In that case, we have the universal single-atom Hamiltonian

$$\hat{H}_1 = -\hbar\Delta_{\text{eff}}|r\rangle\langle r| + \frac{\hbar\Omega_{\text{eff}}}{2}(|r\rangle\langle 1| + |1\rangle\langle r|). \quad (2)$$

For the one-photon ultraviolet excitation, $\Omega_{\text{eff}} = \Omega_{1r}$, $\Delta_{\text{eff}} = \Delta_{1r}$. In the two-photon case $\Omega_{\text{eff}} = (\Omega_{1a}\Omega_{ar})/(2\Delta_{1a})$ and $\Delta_{\text{eff}} = \Delta_{1a} + \Delta_{ar} + (\delta_1 + \delta_r)$, where $\delta_1 = (\Omega_{1a}^2)/(4\Delta_{1a})$ and $\delta_r = -(\Omega_{ar}^2)/(4\Delta_{ar})$ are the light shifts of levels $|1\rangle$ and $|r\rangle$, respectively, due to their coupling to $|a\rangle$. Finally, the entangling two-atom Hamiltonian is

$$\begin{aligned} \hat{H}_{1,1} &= |1\rangle\langle 1| \otimes \hat{H}_1 + \hat{H}_1 \otimes |1\rangle\langle 1| + V|r, r\rangle\langle r, r| \\ &= -\hbar\Delta_{\text{eff}}(|b\rangle\langle b| + |d\rangle\langle d|) \\ &\quad + (V - 2\hbar\Delta_{\text{eff}})|r, r\rangle\langle r, r| \\ &\quad + \frac{\hbar}{2}\sqrt{2}\Omega_{\text{eff}}(|b\rangle\langle 1, 1| + |r, r\rangle\langle b| + \text{H.c.}), \end{aligned} \quad (3)$$

where V is the atom-atom potential energy arising from the EDDI when both atoms are in $|r\rangle$ and $|b\rangle \equiv (|1, r\rangle + |r, 1\rangle)/\sqrt{2}$, $|d\rangle \equiv (|1, r\rangle - |r, 1\rangle)/\sqrt{2}$ are the bright and dark states, respectively, for symmetric coupling [32,37,54]. When $|V| \gg \hbar\Omega_{\text{eff}}, \hbar|\Delta_{\text{eff}}|$, excitation to the doubly excited Rydberg state is strongly blocked. In that case we can reduce this Hamiltonian to a two-atom, two-level system

$$\hat{H}_{1,1} \approx -\hbar\Delta_{\text{eff}}|b\rangle\langle b| + \frac{\hbar}{2}\sqrt{2}\Omega_{\text{eff}}(|b\rangle\langle 1, 1| + |1, 1\rangle\langle b|). \quad (4)$$

The effect of the blockade is seen explicitly in the driving of $|1, 1\rangle$ to the entangled bright state $|b\rangle$.

The eigenstates of the Hamiltonian in Eq. (1) are the dressed states. In particular, we denote the dressed clock states (computational basis states) $\{|0, 0\rangle, |0, \tilde{1}\rangle, |\tilde{1}, 0\rangle, |\tilde{1}, 1\rangle\}$. The eigenvalues $E_{0,\tilde{1}} = E_{\tilde{1},0}$ and $E_{\tilde{1},\tilde{1}}$ contain contributions from light shifts, $E_{\text{LS}}^{(1)}$ with one atom or $E_{\text{LS}}^{(2)}$ with two atoms coupled to the Rydberg state. The entangling energy, denoted by $\hbar\kappa$, is the energy difference between the interacting and noninteracting atoms

$$\begin{aligned} \kappa &= \frac{1}{\hbar}(E_{\text{LS}}^{(2)} - 2E_{\text{LS}}^{(1)}) \\ &\approx \frac{\Delta_{\text{eff}}}{2} \pm \frac{1}{2}(\sqrt{2\Omega_{\text{eff}}^2 + \Delta_{\text{eff}}^2} - 2\sqrt{\Omega_{\text{eff}}^2 + \Delta_{\text{eff}}^2}), \end{aligned} \quad (5)$$

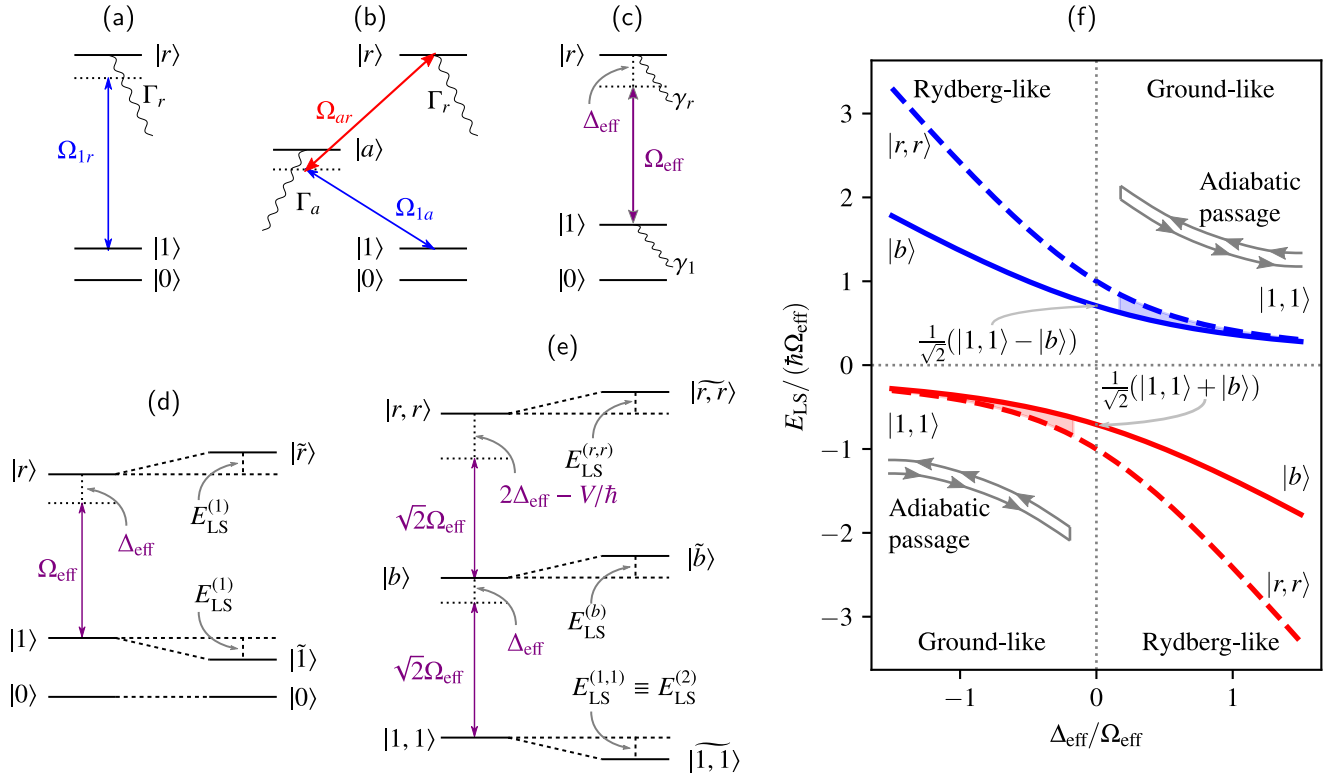


FIG. 1. Two-atom energy levels for implementing adiabatic Rydberg dressing. (a) One-photon $|1\rangle \leftrightarrow |r\rangle$ transition, with Rabi frequency Ω_{1r} and Rydberg decay rate Γ_r . (b) Two-photon $|1\rangle \leftrightarrow |a\rangle \leftrightarrow |r\rangle$ transition with Rabi frequencies Ω_{1a} and Ω_{ar} , respectively, intermediate state decay rate Γ_a and Rydberg decay rate Γ_r . (c) Effective three-level system in regime of adiabatically eliminating the intermediate state $|a\rangle$, with effective Rabi frequency Ω_{eff} and effective detuning Δ_{eff} due to the difference of light shifts experienced by $|a\rangle$ and $|r\rangle$ and effective decay rate γ_r from $|r\rangle$ and γ_1 from $|1\rangle$. (d) Energy levels and light shifts in one-atom dressing, where each atom is dressed independently. (e) Energy levels and light shifts in two-atom dressing, where both atoms are dressed together in the presence of interaction energy V . (f) Energy shifts of atomic states as a function of detuning, in the strong blockade ($\hbar\Omega_{1r} \ll |V|$, $\hbar|\Delta_{1r}| \ll |V|$) case, which play a role in the adiabatic passage between ground-like states and Rydberg-like states. The shaded region shows the entangling energy [5], which is used to accumulate the entangling phase.

where the approximation in the second line holds only in the limit of a perfect blockade, with entangling Hamiltonian Eq. (4) and \pm refers to the two branches of the dressed states in Fig. 1.

An entangling gate is achieved through the dynamical phase accumulated from the entangling energy $\varphi_2 = \int \kappa(t') dt'$ [29,32,37,43,47,55]. As discussed in Ref. [37], we consider generating a two-qubit entangling gate using a spin-echo sequence, as shown in Fig. 2 and demonstrated in Refs. [29,43]. The echo sequence consists of a $\pi/2$ pulse about the x axis, followed by an adiabatic ramp accumulating

nonlocal phase $\varphi_2 = \int \kappa(t') dt'$, an echo a π pulse about the x axis, followed by another adiabatic ramp accumulating nonlocal phase $\varphi_2 = \int \kappa(t') dt'$, and a final $\pi/2$ pulse about the x axis, as shown in Fig. 2(a). An equivalent circuit diagram with the shorthand \sqrt{X} representing a $\pi/2$ pulse about the x axis, X representing a π pulse about the x axis and $\hat{U}_\kappa(\varphi_1, \varphi_2)$ representing the unitary

$$\hat{U}_\kappa(\varphi_1, \varphi_2) = \exp\left[-i\varphi_2\left(\frac{\hat{\sigma}_z}{2} \otimes \frac{\hat{\sigma}_z}{2}\right)\right] \times \exp\left[-i\varphi_1\left(\mathbb{1} \otimes \frac{\hat{\sigma}_z}{2} + \frac{\hat{\sigma}_z}{2} \otimes \mathbb{1}\right)\right], \quad (6)$$

implemented during each adiabatic ramp, is shown in Fig. 2(b). Importantly, the spin-echo removes all phases φ_1 arising for single-atom light shifts, including the dominant errors arising from atom thermal motion and the resulting inhomogeneities [29,37,43]. Designing the adiabatic ramps such that $\varphi_2 = \pi/2$ in each ramp, the resulting unitary transformation is a Mølmer-Sørensen YY gate (MS_{yy}),

$$\hat{U}_{\text{MS}_{yy}} = \exp\left(-\frac{i\pi}{4}\hat{\sigma}_y \otimes \hat{\sigma}_y\right), \quad (7)$$

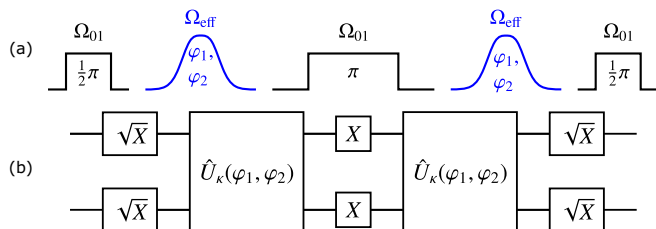


FIG. 2. Adiabatic passages interleaved in a spin-echo sequence. (a) Pulse and ramp sequence. (b) Equivalent circuit diagram. When $\varphi_2 = \pi/2$ the result is the MS_{yy} gate [Eq. (7)].

which is a perfect entangler for the qubits, that is, a gate that can output maximally entangled states from input product states [37,56,57]. This robust protocol extends to two-photon excitation. Off-resonant coupling to the intermediate state leads to additional light shifts and potential noise due to intensity fluctuations. The spin echo removes this noise in its contribution to the single-atom light shift. There will still be some residual error that remains and cannot be canceled in the spin echo, but this is minimal and in practice can be reduced with further robust control techniques.

The fundamental source of decoherence is due to the decay of the Rydberg state at rate Γ_r and the intermediate state at rate Γ_a . To good approximation, the decays will lead to leakage outside the qubit subspace. In that case we can treat decoherence simply through a non-trace-preserving Schrödinger evolution with a non-Hermitian Hamiltonian $\hat{H}_{\text{eff}} = \hat{H} - \frac{i\hbar}{2} \sum_{\mu} \hat{L}_{\mu}^{\dagger} \hat{L}_{\mu}$, where $\{\hat{L}_{\mu}\}$ are the Lindblad jump operators. In the one-photon excitation, $\sum_{\mu} \hat{L}_{\mu}^{\dagger} \hat{L}_{\mu} = \Gamma_r |r\rangle\langle r|$

for each atom. In the two-photon excitation

$$\sum_{\mu} \hat{L}_{\mu}^{\dagger} \hat{L}_{\mu} = \gamma_1 |1\rangle\langle 1| + \gamma_r |r\rangle\langle r| + \gamma_{1r} (|r\rangle\langle 1| + |1\rangle\langle r|), \quad (8)$$

for each atom. Here levels $|1\rangle$ and $|r\rangle$ and their coherences decay due to off-resonant photon scattering with rates

$$\gamma_1 = \frac{\Omega_{1a}^2}{4\Delta_{1a}^2} \Gamma_a, \quad \gamma_r = \frac{\Omega_{ar}^2}{4\Delta_{ar}^2} \Gamma_a + \Gamma_r, \quad \gamma_{1r} = \frac{\Omega_{ra}\Omega_{1a}}{4\Delta_{1a}^2} \Gamma_a. \quad (9)$$

High-fidelity gates for two-photon excitation require sufficiently long lifetimes of level $|a\rangle$.

As studied in Ref. [37], the highest fidelity gates are achieved for strong dressing, with the exciting laser close to Rydberg resonance, and a large admixture of $|b\rangle$ in the dressed state $|1, 1\rangle$. For a one-photon transition, we consider an adiabatic sweep involving a Gaussian laser intensity sweep and the linear detuning sweep, according to

$$\begin{aligned} |\Delta_{1r}(t)| &= \begin{cases} \Delta_{\max} + \frac{\Delta_{\max} - \Delta_{\min}}{t_2 - t_1} \times (t - t_1), & t_1 \leq t < t_2, \\ \Delta_{\min}, & t_2 \leq t \leq t_3, \\ \Delta_{\min} + \frac{\Delta_{\min} - \Delta_{\max}}{t_4 - t_3} \times (t - t_3), & t_3 < t \leq t_4, \end{cases} \\ \Omega_{1r}(t) &= \begin{cases} \Omega_{\min} + (\Omega_{\max} - \Omega_{\min}) \exp\left(-\frac{(t-t_1)^2}{2\tau_w^2}\right), & t_1 \leq t < t_2, \\ \Omega_{\max}, & t_2 \leq t \leq t_3, \\ \Omega_{\min} + (\Omega_{\max} - \Omega_{\min}) \exp\left(-\frac{(t-t_3)^2}{2\tau_w^2}\right), & t_3 < t \leq t_4. \end{cases} \end{aligned} \quad (10)$$

The resulting MS gate was demonstrated in Refs. [29,43].

For the two-photon case, the effect of the light shift arising from the intermediate detuning affords additional possibilities for coherent control. We consider the case of exact two-photon resonance in the absence of the light shift and a fixed Rabi frequency Ω_{ar} and detuning Δ_{ar} on the $|a\rangle \leftrightarrow |r\rangle$ transition. Adiabatic dressing is achieved solely through a Gaussian ramp of the intensity of the laser driving the $|1\rangle \leftrightarrow |a\rangle$ according to the Rabi frequency

$$\Omega_{1a} = \begin{cases} \Omega_{1a}^{\max}, & -|t_{\text{stop}}| \leq t \leq |t_{\text{stop}}|, \\ \Omega_{1a}^{\max} \exp\left(-\frac{(t-|t_{\text{stop}}|)^2}{2\tau_w^2}\right), & \text{otherwise.} \end{cases} \quad (11)$$

One can modulate $|t_{\text{stop}}|$, the time after which the Rabi frequency remains constant, and τ_w the width of the Gaussian pulse, to obtain the desired gate of interest. Figure 3 shows an example of ramps for the two-photon adiabatic passage as well as the population as a function of time during the pulse sequence.

As discussed above, to implement the Mølmer-Sørensen gate we consider two adiabatic ramps intertwined by the spin echo sequence as shown in Fig. 2, similar to that in Ref. [37]. The adiabatic ramps are obtained by numerically maximizing the fidelity defined using the Hilbert-Schmidt overlap

$$\mathcal{F}[\{c_r\}] = \frac{1}{16} |\text{tr}(\hat{U}_{\text{MS}}^{\dagger} \hat{U}(\{c_r\}))|^2, \quad (12)$$

with respect to ramp parameters $\{c_r\}$ for both one photon and two photon cases; here $\hat{U}(\{c_r\})$ is the unitary map imple-

mented using the spin-echo sequence in Fig. 2. Replacing \hat{H} with \hat{H}_{eff} gives an estimate of the fidelity including effects of finite lifetimes of the intermediate state $|a\rangle$ and the Rydberg state $|r\rangle$.

The short lifetime of the intermediate state $|a\rangle$ poses a challenge for implementing adiabatic passage using a two-photon schemes. We explore the dependence of the achievable Mølmer-Sørensen gate fidelity on the intermediate state lifetime and the Rabi frequency in Fig. 4. We fix the Rydberg state decay rate Γ_r , vary the maximum Rabi frequency Ω_{1a}^{\max} and the intermediate state decay rate Γ_a , and then optimize over the intermediate state detuning $\Delta_{1a} = -\Delta_{ar}$ to maximize the fidelity. As in the other two-photon approaches, the choice of an intermediate state with a larger lifetime gives a higher fidelity as this is the fundamental source of error in the model. Moreover, as expected, a larger power gives higher fidelity, but in the perfect blockade regime this is constrained by $\hbar\Omega_{\text{eff}} \ll |V|$. With reasonable experimental parameters, one can achieve fidelity larger than 0.99 as seen in Fig. 4.

A key metric quantifying the temporal duration of the adiabatic Rydberg dressing passages is the time-integrated Rydberg population, summed over both atoms t_r [3,4]. In order for the loss of fidelity due to Rydberg state decay to be small, we require $t_r \ll \tau_r$ where $\tau_r = 1/\Gamma_r$ is the Rydberg-state lifetime [37]. For one-photon adiabatic passages, we found $t_r \approx 0.89 \times 2\pi/\Omega_{\text{eff}}^{\max}$, while for the two-photon passage, we find $t_r \approx 0.95 \times 2\pi/\Omega_{\text{eff}}^{\max}$, with initial state $|1, 1\rangle$. Initial states $|0, 1\rangle$ and $|1, 0\rangle$ lead to smaller time-integrated Rydberg population and initial $|0, 0\rangle$ does not lead to any

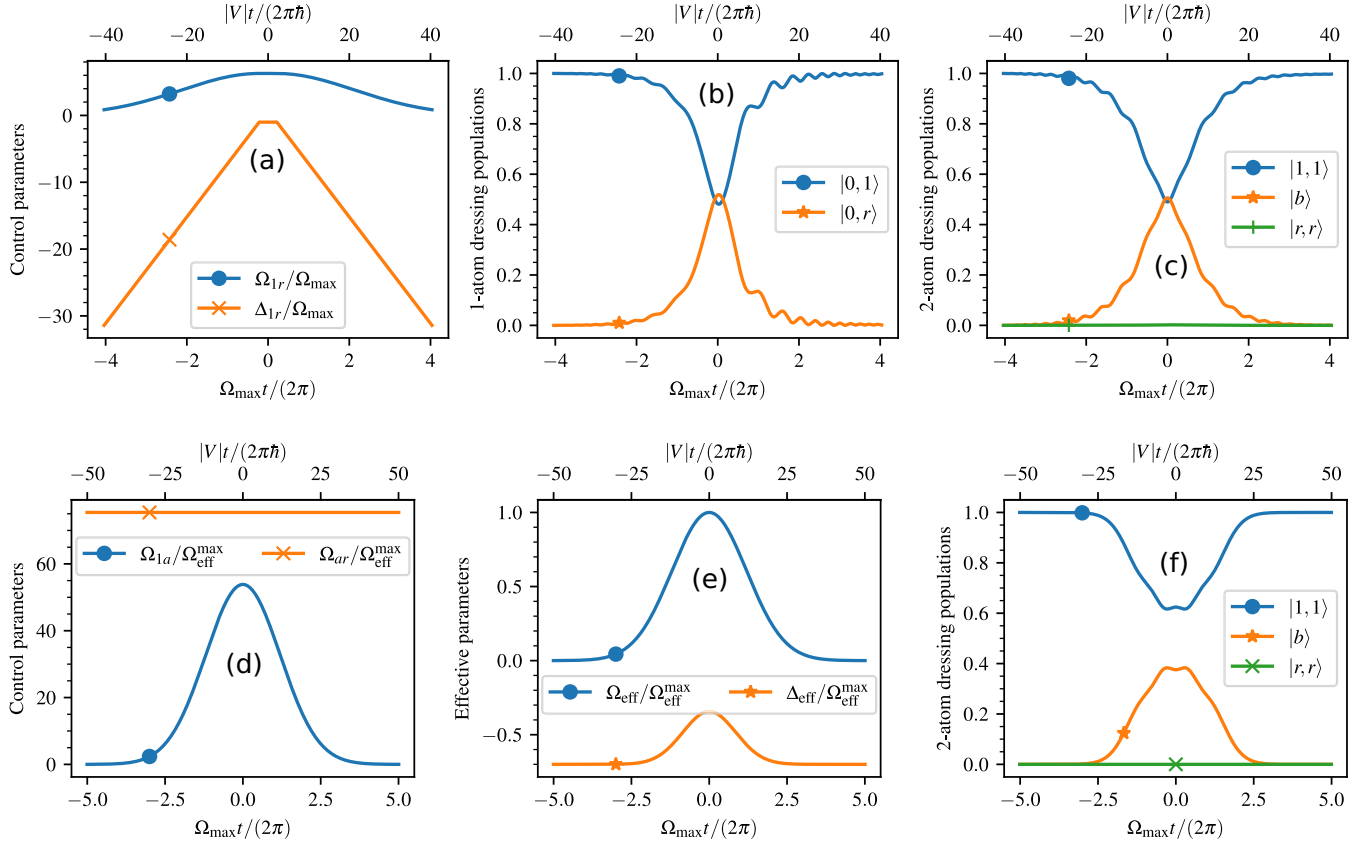


FIG. 3. Adiabatic passages to implement $\hat{U}_\kappa(\varphi_1, \varphi_2)$ with $\varphi_2 = \pi/2$ [Eq. (6), Fig. 2] in the strong blockade regime ($\hbar\Omega_{\text{eff}} = 0.1|V|$). (a) One-photon adiabatic passage Gaussian sweep of Rabi frequency and linear sweep of detuning as in Refs. [37,43]. (b) One-atom populations during a one-photon adiabatic passage. (c) Two-atom population during a one-photon adiabatic passage. (d) Two-photon adiabatic passage using a Gaussian sweep of Rabi frequency Ω_{1a} , with all other parameters fixed, which leads to an effective sweep of the two-photon Rabi frequency Ω_{eff} and two-photon detuning Δ_{eff} as shown in (e). (f) Two-atom populations during a two-photon adiabatic passage. Bottom axes show time measured in units of $2\pi/\Omega_{\text{max}}$, top axes show time measured in units of $|V|t/(2\pi\hbar)$. In the strong blockade, as expected, $|V|t/\hbar \gg \Omega_{\text{max}}t$

Rydberg population [37]. In both one- and two-photon cases, since we are considering the strong blockade regime, the adiabatic passages t_r is significantly larger than $2\pi\hbar/|V|$, the timescale set by the interaction energy V . Nevertheless, using finely tuned parameters, adiabatic Rydberg dressing passages can be used to implement high-fidelity entangling gates.

III. DRESSING BEYOND THE PERFECT BLOCKADE REGIME

In the previous section, we studied entangling gates in the case of a perfect Rydberg blockade, but this is not intrinsic to the adiabatic dressing protocol. Relaxing this assumption and studying protocols in the weak blockade regime is important to address the fundamental limits of Rydberg-atom quantum information processing, potentially improving the fidelity of our gates, and allow us to operate in new regimes. We note that, in practice, quantum fluctuations in the atoms' motional states always affects the fidelity of the implemented gate. The way in which this uncertainty causes gate infidelity depends on the particular protocol. If atoms are released from a trap and are in free fall during the gate (as is commonly the case), the uncertainty in momentum can lead to Doppler shifts and the uncertainty in position can lead to fluctuations in the

atom-atom coupling strength. In principle, atoms can be cooled very close to the motional ground state of a sufficiently deep trap (a nearly pure state) and for some atomic species and specially chosen transitions the gate can be done with the trap on. If the motional state of the atom is not entangled with the internal state, there will be no error arising for the position and momentum uncertainty. Loss of gate fidelity due to atomic motion, arising from uncertainties in position and momentum of the atoms were considered in Refs. [32,37,54].

In addition to the limitations due to uncertainties in atomic motional states, no matter how cool the atoms are or how well we can remove these effects by special protocols, implementation of an entangling gate using Rydberg-mediated interactions is fundamentally limited by two energy timescales: the Rydberg-state lifetime τ_r and the magnitude of the interatomic interaction energy $|V|$ [3,4]. Wesenberg *et al.* showed that the minimum time that the atoms need to spend in a Rydberg state to achieve a maximally entangling gate scales as $t_r \sim \hbar/|V|$ [51]. The standard protocols which employ a strong Rydberg blockade [5,30] cannot achieve this bound because the speed of the gates is set by Ω_{eff} , and since they require $\hbar\Omega_{\text{eff}} \ll |V|$, we cannot make use of the full scale of the interaction energy [3]. Jo *et al.* implemented Rydberg-mediated entanglement outside

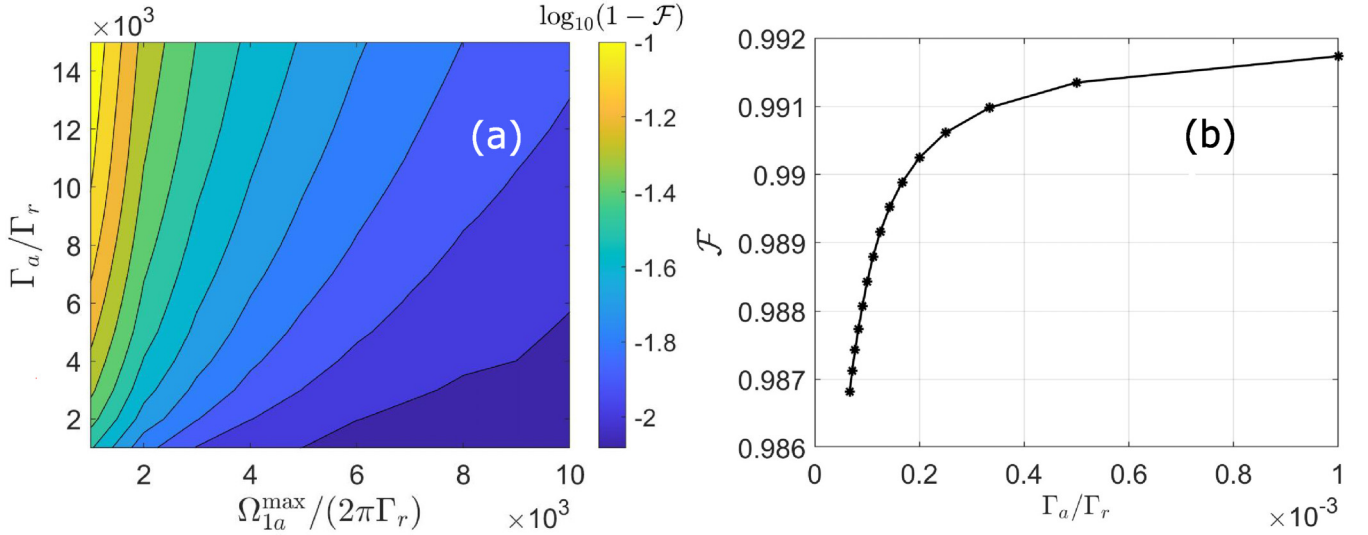


FIG. 4. Dependence of the fidelity of the Mølmer-Sørensen gate on the intermediate state decay rate Γ_a and the Rabi frequency Ω_{1a} , both measured in units of the Rydberg state decay rate Γ_r . Similar to other two-photon approaches the choice of intermediate state with smaller decay rate gives a better fidelity. Moreover, as expected, a larger power gives better fidelity. However, this gives us the constraint that we need a larger $|V|$ and thus poses some additional challenges. With a reasonable experimental parameters one could achieve an infidelity less than 10^{-2} . The data are obtained by fixing the ratios Γ_a/Γ_r and $\Omega_{1a}^{\max}/(2\pi\Gamma_r)$ and optimizing over the choice of the detuning from the intermediate state $\Delta_{1a} = -\Delta_{ar}$. (a) Contour plot of the logarithm of infidelity, $\log_{10}(1 - \mathcal{F})$ across different values of Γ_a/Γ_r and $\Omega_{1a}^{\max}/(2\pi\Gamma_r)$. (b) Fidelity, \mathcal{F} as a function of the ratio Γ_a/Γ_r , for $\Omega_{1r} = 1.4\Omega_{1a}^{\max}$ and $\Omega_{1a}^{\max}/(2\pi\Gamma_r) = 10^4$.

the strong blockade regime using finely tuned two-atom Rabi oscillations [42].

The minimum timescale for t_r can be understood in a simple protocol using the limiting case of a very large Rabi frequency $\hbar\Omega_{\text{eff}}^{\max}/|V| \rightarrow \infty$. An entangling gate can be achieved using a collective π pulse from $|1\rangle$ to $|r\rangle$ on both atoms, followed by an interaction for a time $|V|t_r/\hbar = \pi$ and a π pulse from $|r\rangle$ to $|1\rangle$. In the limit of infinitesimally short π pulses, the time spent in Rydberg states, or time-integrated Rydberg population, is $\pi\hbar/|V|$. All of the time spent in the Rydberg states is in the doubly excited Rydberg state $|r, r\rangle$.

While this simple protocol helps us understand the timescales, it is generally not practical for implementation. For small interatomic separations, the two-atom spectrum becomes a complex tangle of ‘‘Rydberg spaghetti’’ [47,50]. To achieve the fastest gates in this strongly interacting case, it is thus useful to avoid double Rydberg population which can lead to unexpected inelastic processes. In addition, the complex potential landscape at such small interatomic separations can lead to high sensitivity to atomic motion. In this section we show that using adiabatic Rydberg dressing, we can get close to the minimum timescale t_r , while working in the weak blockade regime, $\hbar\Omega_{\text{eff}}^{\max} \gg |V|$, without significant double Rydberg population. Moreover, for large interatomic separations, protocols requiring a strong blockade would lead to exceedingly slow gates. The adiabatic dressing protocol considered here can achieve reasonably fast gates with high fidelity, even for atoms separated beyond blockade radius.

To understand the different regimes of operation, we estimate how the interatomic interaction energy V limits the entangling energy $\hbar\kappa$ in the strong blockade and weak blockade regimes. For simplicity, we consider the case in which the atoms see the same Rabi frequency, given in Eq. (3). It

is useful to consider a pseudospin with $|\uparrow_z\rangle \equiv |r\rangle$ and $|\downarrow_z\rangle \equiv |1\rangle$. Note that this is different from the dressed pseudospin considered in Refs. [29,37,43], where the pseudospin levels corresponded to the dressed ground states. In this pseudospin picture, the two-atom Hamiltonian can be written as a sum of two terms

$$\begin{aligned} \hat{H}_{\text{int}} &= V|r, r\rangle\langle r, r| \equiv \frac{V}{2}(\hat{S}_z^2 + \hat{S}_z), \\ \hat{H}_{\text{drive}} &\equiv -\hbar\Delta_{\text{eff}}\mathbb{1} - \hbar\Delta_{\text{eff}}\hat{S}_z + \hbar\Omega_{\text{eff}}\hat{S}_x \\ &\equiv -\hbar\Delta_{\text{eff}}\mathbb{1} + \hbar\sqrt{\Delta_{\text{eff}}^2 + \Omega_{\text{eff}}^2}\hat{S}_\theta, \end{aligned} \quad (13)$$

where \hat{S}_μ is the μ component of collective angular momentum operator $S_\mu = \mathbb{1} \otimes \hat{\sigma}_\mu/2 + \hat{\sigma}_\mu/2 \otimes \mathbb{1}$, $\hat{S}_\theta = \cos\theta\hat{S}_z + \sin\theta\hat{S}_x$ with $\tan\theta = \Omega_{\text{eff}}/(-\Delta_{\text{eff}})$. The collective symmetric spin-1 eigenstates of S_z are the triplet of the pseudospins $|S=1, M_z=-1\rangle = |1, 1\rangle$, $|S=1, M_z=0\rangle = (|1, r\rangle + |r, 1\rangle)/\sqrt{2} = |b\rangle$, $|S=1, M_z=+1\rangle = |r, r\rangle$. The eigenvalues and eigenvectors of the driving Hamiltonian and

TABLE I. Eigenvalues and eigenvectors of the atom-light Hamiltonian \hat{H}_{drive} . Here $|\uparrow_\theta\rangle \equiv \cos(\theta/2)|\uparrow_z\rangle + \sin(\theta/2)|\downarrow_z\rangle$, $|\downarrow_\theta\rangle \equiv \cos(\theta/2)|\downarrow_z\rangle - \sin(\theta/2)|\uparrow_z\rangle$, and $\tan\theta = \Omega_{\text{eff}}/(-\Delta_{\text{eff}})$. The first two rows represent the upper and lower branches of the single-atom dressed states.

Energy eigenvalue	Eigenvectors
$-\hbar\Delta_{\text{eff}} + \hbar\sqrt{\Omega_{\text{eff}}^2 + \Delta_{\text{eff}}^2}$	$ \uparrow_\theta\rangle \otimes \uparrow_\theta\rangle$
$-\hbar\Delta_{\text{eff}} - \hbar\sqrt{\Omega_{\text{eff}}^2 + \Delta_{\text{eff}}^2}$	$ \downarrow_\theta\rangle \otimes \downarrow_\theta\rangle$
$-\hbar\Delta_{\text{eff}}$	$(\uparrow_\theta\rangle \otimes \downarrow_\theta\rangle + \downarrow_\theta\rangle \otimes \uparrow_\theta\rangle)/\sqrt{2}$

TABLE II. Eigenvalues and eigenvectors of the atom-atom interaction Hamiltonian \hat{H}_{int} in the symmetric subspace, spanned by $|1, 1\rangle, |b\rangle, |r, r\rangle$.

Energy eigenvalue	Eigenvectors
V	$ r, r\rangle$
0	$ b\rangle, 1, 1\rangle$

the interaction Hamiltonian are in Tables I and II, respectively.

First, we consider the well-known strong blockade regime with $|V| \gg \hbar\Omega_{\text{eff}}$, where the interaction term is the dominant Hamiltonian and the driving term is the perturbation. The zeroth-order eigenvectors are the states $|S = 1, M_z\rangle$. The leading-order correction is calculated using degenerate perturbation theory in the zero eigenvalue subspace spanned by $|S = 1, M_z = -1\rangle \equiv |1, 1\rangle$ and $|S = 1, M_z = 0\rangle \equiv |b\rangle$. The eigenvalues and corresponding eigenvectors of \hat{S}_θ in the zero-eigenvalue subspace of \hat{H}_{int} are in Table III. Using \mathcal{P}_{S, M_z} to denote the projector on the subspace of S, M_z ,

$$\begin{aligned} & (\mathcal{P}_{S=1, M_z=-1} + \mathcal{P}_{S=1, M_z=0})\hat{S}_\theta, (\mathcal{P}_{S=1, M_z=-1} + \mathcal{P}_{S=1, M_z=0}) \\ &= -\cos(\theta)|S = 1, M_z = -1\rangle\langle S = 1, M_z = -1| \\ &+ \frac{\sin(\theta)}{\sqrt{2}}(|S = 1, M_z = -1\rangle\langle S = 1, M_z = 0| \\ &+ \frac{\sin(\theta)}{\sqrt{2}}(|S = 1, M_z = 0\rangle\langle S = 1, M_z = -1|). \quad (14) \end{aligned}$$

The perturbative corrections to energy eigenvalues are the two-atom light shift experienced by the atoms together in the presence of V . The leading correction to the energy of the logical state $|1, 1\rangle \equiv |S = 1, M_z = -1\rangle$ in perturbation theory, is the two-atom light shift under perfect blockade

$$E_{\text{LS}}^{(2)} = -\frac{\hbar\Delta_{\text{eff}}}{2} \pm \frac{\hbar}{2}\sqrt{2\Omega_{\text{eff}}^2 + \Delta_{\text{eff}}^2}. \quad (15)$$

Subtracting out the energy shifts in eigenstates of each atom to obtain the entangling energy κ using Eq. (5),

$$\begin{aligned} & \lim_{\hbar\Omega_{\text{eff}}/|V| \rightarrow 0} \kappa \\ &= -\frac{\Delta_{\text{eff}}}{2} \pm \frac{1}{2}(\sqrt{\Delta_{\text{eff}}^2 + 2\Omega_{\text{eff}}^2} - 2\sqrt{\Delta_{\text{eff}}^2 + \Omega_{\text{eff}}^2}). \quad (16) \end{aligned}$$

Note that, here by design, $\hbar|\kappa| \ll |V|$ since we assumed $\hbar\Omega_{\text{eff}} \ll |V|$. The maximum useful κ scales with the Rabi frequency Ω_{eff} . Under a perfect Rydberg blockade regime

TABLE III. Eigenvalues and eigenvectors of \hat{S}_θ in the zero-eigenvalue subspace of \hat{H}_{int} . Here, $\tan \Theta = \sqrt{2}\Omega_{\text{eff}}/(-\Delta_{\text{eff}})$. The upper and lower rows represent the upper and lower branches of the two-atom dressed states in the perfect blockade regime, shown in Fig. 1.

Energy eigenvalue	Eigenvectors
$-\frac{1}{2}\cos\theta + \frac{1}{2}\sqrt{\cos^2\theta + 2\sin^2\theta}$	$\cos\frac{\Theta}{2} b\rangle + \sin\frac{\Theta}{2} 1, 1\rangle$
$-\frac{1}{2}\cos\theta - \frac{1}{2}\sqrt{\cos^2\theta + 2\sin^2\theta}$	$\cos\frac{\Theta}{2} 1, 1\rangle - \sin\frac{\Theta}{2} b\rangle$

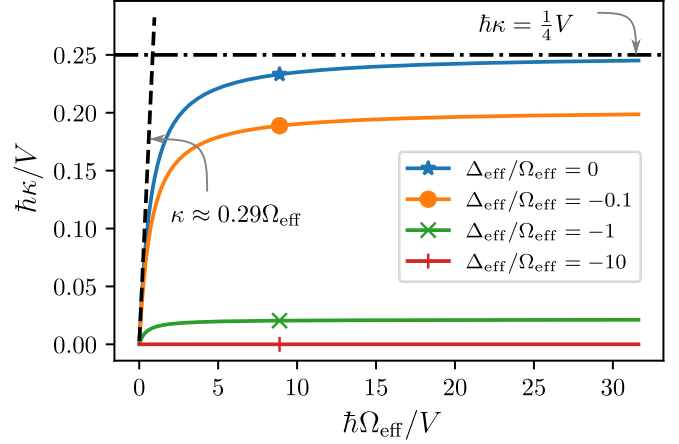


FIG. 5. Entangling energy in units of the interaction energy as a function of the ground to Rydberg Rabi frequency in units of the interaction energy for different detunings. For small detunings, in the strong blockade regime $\hbar\Omega_{\text{eff}} \ll |V|$, the entangling energy scales linearly the Rabi frequency, and in the weak blockade regime $\hbar\Omega_{\text{eff}} \gg |V|$, the entangling energy is independent of the Rabi frequency and scales linearly with the interaction energy. For large detunings, the entangling energy is negligible.

$|V| \gg \hbar\Omega_{\text{eff}}$, the state $|r, r\rangle$ is not populated. Thus, there is an adiabatic passage from the $|1, 1\rangle$ to $|b\rangle$ and back as shown in Fig. 1(f).

Next, we consider the weak blockade regime where $|V| \ll \hbar\Omega_{\text{eff}}$. In this case, the laser-driving term is the dominant Hamiltonian and the interaction term is a perturbation. The eigenstates of the driving Hamiltonian are the one-atom dressed states, which are rotated spin-triplet states $|S = 1, M_\theta\rangle$ given in Table I. The energy eigenvalues are the one-atom light shift. The entangling energy $\hbar\kappa$ can be estimated as the correction to the dressed ground state $|\bar{1}, 1\rangle \equiv |S = 1, M_\theta = -1\rangle \equiv (\cos\frac{\theta}{2}|1\rangle + \sin\frac{\theta}{2}|r\rangle)^{\otimes 2}$. The unperturbed energies of the dominant Hamiltonian include the single-atom light shifts. Therefore, the leading-order correction to the noninteracting energy is the asymptotic value of $\hbar\kappa$,

$$\lim_{|V|/\hbar\Omega_{\text{eff}} \rightarrow 0} \hbar\kappa = \left(\frac{1 \pm \cos\theta}{2}\right)^2 V, \quad (17)$$

where \pm refers to the relative sign of the initial detuning and the detuning at peak dressing during an adiabatic passage and the corresponding (unnormalized) dressed state, in leading-order perturbation theory, is

$$\begin{aligned} & |\widetilde{1}, 1\rangle \equiv \left(\cos\frac{\theta}{2}|1\rangle + \sin\frac{\theta}{2}|r\rangle\right)^{\otimes 2} \\ & \pm \cos^2\left(\frac{\theta}{2}\right) \frac{V}{2\hbar\sqrt{\Omega_{\text{eff}}^2 + \Delta_{\text{eff}}^2}} |r, r\rangle, \quad (18) \end{aligned}$$

now including the doubly excited Rydberg state.

We calculate the entangling energy $\hbar\kappa$ numerically beyond the perfect blockade regime for different detunings as shown in Fig. 5. We focus on entangling protocols that limit the population in the doubly excited Rydberg state $|r, r\rangle$ to

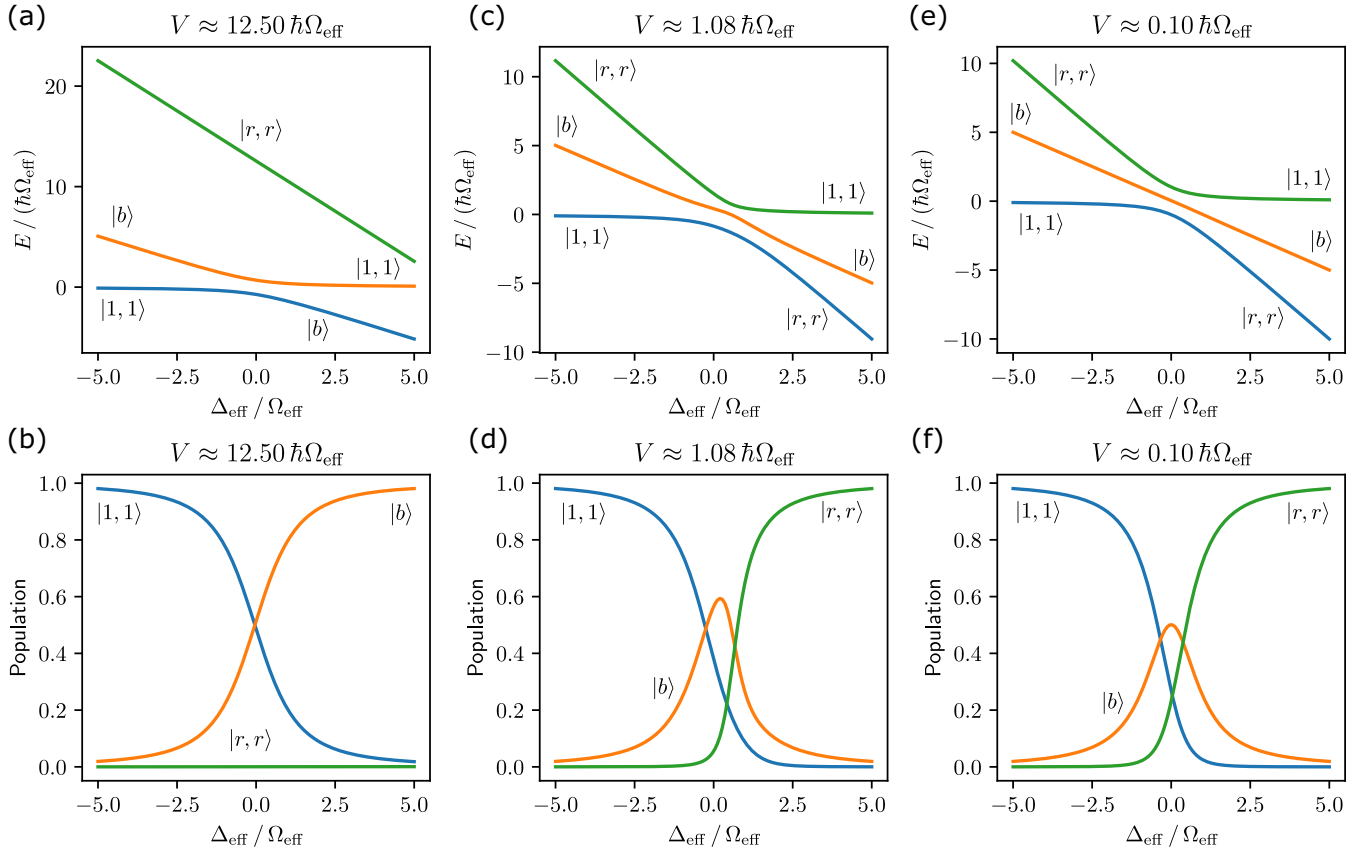


FIG. 6. Dressed state energies and populations in the basis $\{|1, 1\rangle, |b\rangle, |r, r\rangle\}$ as a function of $\Delta_{\text{eff}}/\Omega_{\text{eff}}$ in different blockade regimes. (a), (b) Strong blockade. (c), (d) Intermediate blockade. (e), (f) Weak blockade. (a), (c), and (e) energy eigenvalues V , while (b), (d), and (f) show populations of dressed states, when the initial detuning $\Delta_{\text{eff}} < 0$.

avoid potentially deleterious decay and inelastic processes. To ensure this, we consider adiabatic ramps that are far from the antiblockade condition $V = 2\hbar\Delta_{\text{eff}}$. In practice, this is done in the weak blockade case with a detuning at peak dressing (minimum $|\Delta_{\text{eff}}|$) satisfying $\hbar|\Delta_{\text{eff}}| \ll |V|$. As predicted from perturbation theory, we see that entangling energy scales with the Rabi frequency in the strong blockade regime and reaches $V/4$ at resonance in the weak blockade regime.

Theoretically, all of the interaction energy V is available as the Rydberg dressing entangling energy $\hbar\kappa$. However, this occurs when $\theta \in \{0, \pi\}$ or $|\Delta_{\text{eff}}|/\Omega_{\text{eff}} \rightarrow \infty$ when the dressed state is simply the bare atomic state $|r, r\rangle$. As we saw in Ref. [37], an adiabatic passage that starts far from ground-Rydberg resonance, goes close to resonance, and returns to far off-resonance is most effective at limiting double Rydberg excitation. In this weak blockade case the adiabatic passage stays far from the antiblockade condition, leading to a dressed state $|1, 1\rangle$ that is primarily an admixture of $|1, 1\rangle$ and the bright state $|b\rangle$, with a small $|r, r\rangle$ component.

In Fig. 6 we consider examples of strong ($V \gg \hbar\Omega_{\text{eff}}$), intermediate ($V \sim \hbar\Omega_{\text{eff}}$), and weak ($V \ll \hbar\Omega_{\text{eff}}$), showing the dressing energies and the populations of bare states $|1, 1\rangle, |b\rangle, |r, r\rangle$ in the dressed state $|1, 1\rangle$. Given the energy gaps, we see that the adiabatic dressing protocol allows for a gate as fast as a timescale of $\sim 2\pi\hbar/|V|$, and importantly, by sweeping the detuning close to resonance, while avoiding

the antiblockade condition, there is negligible excitation of the doubly excited Rydberg state $|r, r\rangle$. For example, we study $|V| = 0.1\hbar\Omega_{\text{eff}}$ for both the one- and two-photon excitation; the ramps are shown in Fig. 7 using the same parametrization used for the strong blockade case, Eqs. (10) and (11). Despite the weak blockade, we see that the population accumulated in the state $|r, r\rangle$ is bounded, which overcomes one of the significant hurdles in going beyond perfect blockade.

Let us return to the question of the maximum possible achievable entangling gate fidelity, assuming loss of fidelity due to uncertainties in atomic motion is negligible. When considering adiabatic Rydberg dressing, the entanglement is generated in the form of the dynamical phases from the entangling energy $\int dt' \kappa(t')$ [32,37]. Fundamentally, the time spent in the Rydberg state is bounded by an energyscale proportional to the entangling energy $\hbar\kappa$. Using adiabatic Rydberg dressing in the strong-blockade regime leads to t_r that scales inversely with the Rabi frequency as $\kappa \sim \Omega_{\text{max}}$, and therefore, is far from the minimum, $t_r \sim 2\pi/\Omega_{\text{max}} \gg \pi\hbar/|V|$. In Fig. 8, we plot the time-integrated Rydberg population as a function of the ratio of Rabi frequency to the interatomic Rydberg interaction energy $\hbar\Omega_{\text{eff}}^{\text{max}}/|V|$ for both the one-photon case using Eq. (10) and the two-photon ramps as given in Eq. (11). The analysis indicates that the time-integrated population required to create the perfect entangler, while avoiding the antiblockade condition, decreases as we increase the Rabi

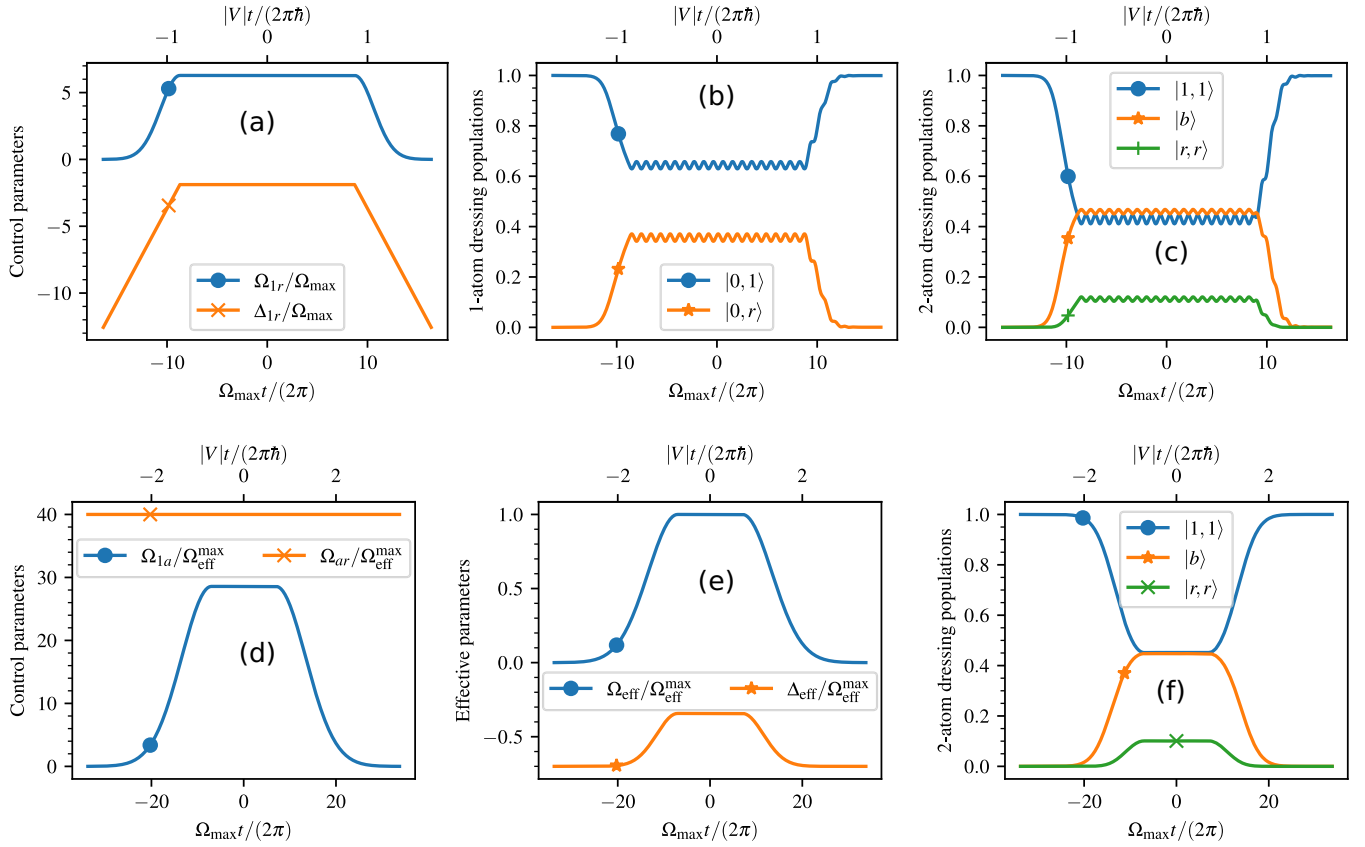


FIG. 7. Adiabatic passages to implement $\hat{U}_\kappa(\varphi_1, \varphi_2)$ with $\varphi_2 = \pi/2$ [Eq. (6), Fig. 2] in the weak blockade regime ($\hbar\Omega_{\text{eff}} = 0.1|V|$). (a) One-photon adiabatic passage Gaussian sweep of Rabi frequency and linear sweep of detuning as in Refs. [37,43]. (b) One-atom populations during a one-photon adiabatic passage. (c) Two-atom populations during a one-photon adiabatic passage. (d) Two-photon adiabatic passage using a Gaussian sweep of Rabi frequency Ω_{1a} , with all other parameters fixed, which leads to an effective sweep of the two-photon Rabi frequency Ω_{eff} and two-photon detuning Δ_{eff} as shown in (e). (f) Two-atom populations during a two-photon adiabatic passage. Bottom axes show time measured in units of $2\pi/\Omega_{\text{max}}$, top axes show time measured in units of $Vt/\hbar \ll \Omega_{\text{max}}t$.

frequency $\hbar\Omega_{\text{max}}$, compared to the interaction energy $|V|$ and it eventually saturates to slightly above $4\pi\hbar/|V|$.

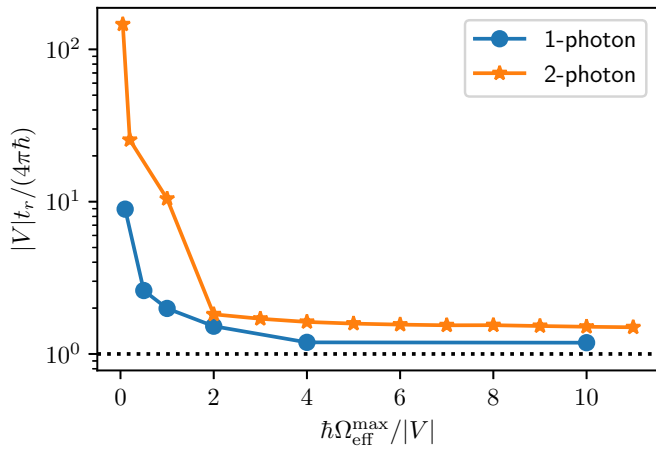


FIG. 8. Time-integrated Rydberg population t_r as a function of Rydberg interaction V for the one- and two-photon ramps. In both cases, the integrated Rydberg population becomes lower and lower as we increase $\hbar\Omega_{\text{eff}}^{\text{max}}/|V|$ for the two-photon adiabatic passage as in Eq. (11) and one-photon adiabatic passage as in Eq. (10).

This result is consistent with the bound found in Ref. [51]. Since the value of $\hbar|\kappa|$ reaches $|V|/4$ near resonance in the weak blockade regime [Eq. (17)], the theoretically achievable maximum fidelity, while the limiting double Rydberg excitation is

$$\mathcal{F} < 1 - \frac{4\pi\hbar}{|V|\tau_r}, \quad (19)$$

where τ_r is the Rydberg-state lifetime. For contemporary experiments, with $|V|/(2\pi\hbar) = 40$ MHz and $\tau_r = 150 \mu\text{s}$, the theoretical minimum infidelity is about 10^{-3} . With cryogenically enhanced Rydberg lifetimes, around $\tau_r = 1$ ms and stronger interactions, $|V|/(2\pi\hbar) = 1$ GHz, the theoretical minimum infidelity would be 10^{-5} . In practice, achieving this would require working in the weak blockade regime, with large laser power such that $\hbar\Omega_{\text{eff}} \gg |V|$.

The ability to design gates with adiabatic dressing beyond the perfect blockade regime also loosens other constraints and potential sources of error. Maintaining atoms beyond the blockade radius reduces the requirement for transporting atoms, which leads to motional heating. Our results show that, even for moderate EDDI, with $|V|/(2\pi\hbar)$ of a few MHz, one can achieve fast gates with gates times of the order of a few μs . Moreover, at moderate separations, the shifted doubly excited states are well resolved and well defined, reducing

spurious resonances. A potential downside to the operation in this regime is the sensitivity of the entangling energy-to-atom separation and also the resulting forces on the atoms. We address this in the Appendix.

IV. CONCLUSION

In this article, we explored some practical considerations and fundamental limits of the adiabatic Rydberg dressing protocol for two-qubit quantum logic gates, where entanglement is generated by the modification of the ground-state light shift introduced by the interaction energy between Rydberg atoms. We studied adiabatic Rydberg dressing via a two-photon ground-to-Rydberg transition and found adiabatic ramps that can be used to achieve high-fidelity entangling gates by modulating only one laser amplitude as a function of time, with all laser frequencies fixed, allowing an easier experimental implementation and alleviating the need for a high-power ultraviolet laser (Sec. II). A major bottleneck for adiabatic Rydberg dressing-based entangling gates in the case of a two-photon ground-to-Rydberg transition is the intermediate-state lifetime. We found that, with current state of the art with Rydberg lifetimes $\sim 100\mu\text{s}$ and ground-to-Rydberg Rabi frequencies $\sim 4\text{MHz}$, gates with fidelity 0.99 are achievable in a regime that adiabatically eliminates the intermediate state, but still maintains reasonable two-photon Rabi frequencies. This protocol is applicable for both alkali and alkaline-earth-like atoms.

We also studied the fundamental limits of implementing an entangling gate using adiabatic Rydberg dressing of ground states, set by the finite Rydberg lifetime and the entangling energy obtained in the dressed states (Sec. III). We showed that, in the well-known strong blockade regime, the entangling energy scale is limited by the ground-Rydberg Rabi frequency, that is, laser power, and in the weak blockade regime, the entangling energy is limited by the interaction energy between the atoms. Moreover, we showed proof-of-principle feasibility of rapid adiabatic passages without significant double-Rydberg population in strong, intermediate, and weak blockade regimes, thereby loosening the requirements of atoms being within a blockade radius for implementing entangling gates in a few μs . A more precise model of the entangling energy using atomic species and Rydberg-state specific treatment, for example, as in Ref. [49], can be used to design adiabatic passages for specific experiments.

In conclusion, adiabatic Rydberg dressing is a promising approach to implementing two-qubit entangling gates for neutral atoms. It can be implemented in several atomic species with one- or two-photon ground-to-Rydberg transitions and can be designed beyond the strong blockade regime to yield fast, high-fidelity gates.

ACKNOWLEDGMENTS

We thank Antoine Browaeys for the fruitful discussions and the anonymous referees for valuable comments. We acknowledge the Pueblo of Sandia, who are the traditional owners and stewards of the land on which the University of New Mexico now sits. This research is supported by the Laboratory Directed Research and Development program of Los Alamos

National Laboratory under Project No. 20200015ER and the NSF Quantum Leap Challenge Institutes program, Award No. 2016244. Los Alamos National Laboratory is managed by Triad National Security, LLC, for the National Nuclear Security Administration of the U.S. Department of Energy under Contract No. 89233218CNA0000.

APPENDIX: QUANTIFYING FORCE ON ATOMS

Outside the strong blockade regime, it is important to consider the interatomic forces that could potentially effect the motional state of the atoms. Two atoms directly excited into the Rydberg state will experience a large van der Waals force from the EDDI. However, in adiabatic dressing a force will arise from the spatial gradient of the light shift, i.e., the “soft core” adiabatic potential force arising from the $|r, r\rangle$ component in the dressed state $|\widetilde{1}, 1\rangle$.

Consider, thus, the adiabatic interatomic potential experienced by atoms in instantaneous internal “adiabatic state” $|\psi(\mathbf{R})\rangle$. We treat here the center-of-mass motion of the atoms classically, in which the interatomic force is given according to

$$V_{\text{ad}} = \langle \psi(\mathbf{R}) | H(\mathbf{R}) | \psi(\mathbf{R}) \rangle \Rightarrow \mathbf{F} = -\nabla V_{\text{ad}}, \quad (\text{A1})$$

where $|\psi(\mathbf{R})\rangle = c_{11}(\mathbf{R})|1, 1\rangle + c_b(\mathbf{R})|b\rangle + c_{rr}|r, r\rangle$. The coefficients depend on the interatomic distance \mathbf{R} . If the state is an eigenstate of H , for example, the adiabatic potential of the dressed ground state $|\widetilde{1}, 1\rangle$ is

$$V_{\text{ad}}(\widetilde{1}, 1) = E(\widetilde{1}, 1) = \hbar\kappa(\mathbf{R}) + 2E_{\text{LS}}^{(1)} + 2E_1, \quad (\text{A2})$$

which gives a force

$$\mathbf{F}(\widetilde{1}, 1) = -\hbar\nabla\kappa(\mathbf{R}), \quad (\text{A3})$$

as the one-atom light shift $E_{\text{LS}}^{(1)}$ and bare energy E_1 are independent of \mathbf{R} .

When the interatomic distance is well within the blockade radius, where we have a perfect blockade, κ is independent of \mathbf{R} . This leads to a “soft-core” potential which was observed

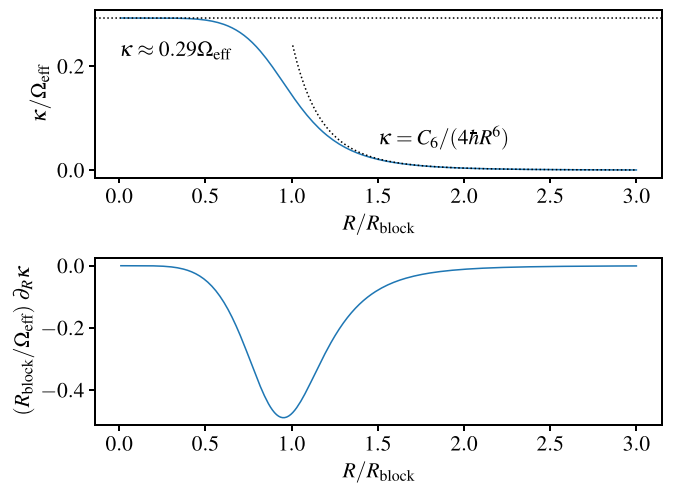


FIG. 9. Interatomic potential energy and forces between atoms in the dressed state $|\widetilde{1}, 1\rangle$. (a) Entangling energy κ in units of the Rabi frequency Ω_{eff} as a function of interatomic distance R , in units of the blockade radius R_{block} . (b) Gradient of the entangling energy along the interatomic direction $\partial_R \kappa$ in units of the ratio $\Omega_{\text{eff}}/R_{\text{block}}$.

experimentally in Refs. [14,15,43,47]. This can also be analyzed on the basis of bare atomic orbitals. For simplicity, consider the case of zero detuning, the adiabatic potential between dressed ground states is

$$V_{\text{ad}}(\widetilde{1}, \widetilde{1}) = \sqrt{2}\Omega_{\text{eff}}\{\text{Re}[c_{11}(\mathbf{R})c_b^*(\mathbf{R})] + \text{Re}[c_{11}(\mathbf{R})c_{rr}^*(\mathbf{R})]\} + |c_{rr}|^2V(\mathbf{R}). \quad (\text{A4})$$

Note the force is not simply $|c_{rr}|^2\nabla V(\mathbf{R})$; the interference terms in the adiabatic potential reduces the otherwise large force.

For simplicity and generality, we calculate κ as a function of distance using a van der Waals potential $V = C_6|\mathbf{R}|^{-6}$ and the interatomic force as a function of distance in Fig. 9. As

is standard, we define the blockade radius where the energy of Rabi frequency of the Rydberg excitation is equal to V , $\hbar\Omega_{\text{eff}} = C_6R_{\text{block}}^{-6}$. At short interatomic distances the adiabatic potential has a soft-core form and is the entangling energy $\hbar\kappa$, up to additive constants, as observed experimentally in Refs. [14,15,43,47]. At large distances, the interatomic potential asymptotes to a quarter of the van der Waals potential, $C_6|\mathbf{R}|^{-6}/4$ for van der Waals interactions. The transition occurs roughly between $|\mathbf{R}|/R_{\text{block}} \approx 1/2$ and $|\mathbf{R}|/R_{\text{block}} \approx 2$, where the potential energy has a nonzero gradient, giving rise to a nontrivial interatomic force (Fig. 9). From these results, we see that the operation of an adiabatic dressing gate outside the perfect blockade regime will lead to bounded perturbing forces on the atoms.

-
- [1] G. K. Brennen, C. M. Caves, P. S. Jessen, and I. H. Deutsch, Quantum Logic Gates in Optical Lattices, *Phys. Rev. Lett.* **82**, 1060 (1999).
- [2] L. Isenhower, E. Urban, X.-L. Zhang, A.-T. Gill, T. Henage, T.-A. Johnson, T.-G. Walker, and M. Saffman, Demonstration of a Neutral Atom Controlled-NOT Quantum Gate, *Phys. Rev. Lett.* **104**, 010503 (2010).
- [3] M. Saffman, T. G. Walker, and K. Mølmer, Quantum information with Rydberg atoms, *Rev. Mod. Phys.* **82**, 2313 (2010).
- [4] M. Saffman, Quantum computing with atomic qubits and Rydberg interactions: progress and challenges, *J. Phys. B: At., Mol. Opt. Phys.* **49**, 202001 (2016).
- [5] H. Levine, A. Keesling, G. Semeghini, A. Omran, T. T. Wang, S. Ebadi, H. Bernien, M. Greiner, V. Vuletić, H. Pichler *et al.*, Parallel Implementation of High-Fidelity Multiqubit Gates with Neutral Atoms, *Phys. Rev. Lett.* **123**, 170503 (2019).
- [6] S. R. Cohen and J. D. Thompson, Quantum computing with circular Rydberg atoms, *PRX Quantum* **2**, 030322 (2021).
- [7] S. Notarnicola, A. Elben, T. Lahaye, A. Browaeys, S. Montangero, and B. Vermersch, A randomized measurement toolbox for Rydberg quantum technologies, *arXiv:2112.11046*.
- [8] A. P. Burgers, S. Ma, S. Saskin, J. Wilson, M. A. Alarcón, C. H. Greene, and J. D. Thompson, Controlling Rydberg excitations using ion-core transitions in alkaline-earth atom-tweezer arrays, *PRX Quantum* **3**, 020326 (2022).
- [9] Y. Wu, S. Kolkowitz, S. Puri, and J. D. Thompson, Erasure conversion for fault-tolerant quantum computing in alkaline earth Rydberg atom arrays, *Nat. Commun.* **13**, 4657 (2022).
- [10] D. Bluvstein, H. Levine, G. Semeghini, T. T. Wang, S. Ebadi, M. Kalinowski, A. Keesling, N. Maskara, H. Pichler, M. Greiner *et al.*, A quantum processor based on coherent transport of entangled atom arrays, *Nature (London)* **604**, 451 (2022).
- [11] T.-M. Graham, Y. Song, J. Scott, C. Poole, L. Phuttitarn, K. Jooya, P. Eichler, X. Jiang, A. Marra, B. Grinkemeyer *et al.*, Multi-qubit entanglement and algorithms on a neutral-atom quantum computer, *Nature (London)* **604**, 457 (2022).
- [12] S. Ebadi, A. Keesling, M. Cain, T. T. Wang, H. Levine, D. Bluvstein, G. Semeghini, A. Omran, J.-G. Liu, R. Samajdar *et al.*, Quantum optimization of maximum independent set using Rydberg atom arrays, *Science* **376**, 1209 (2022).
- [13] S. Jandura, J. D. Thompson, and G. Pupillo, Optimizing Rydberg Gates for Logical-Qubit Performance, *PRX Quantum* **4**, 020336 (2023).
- [14] J. Zeiher, R. Van Bijnen, P. Schauß, S. Hild, J. Y. Choi, T. Pohl, I. Bloch, and C. Gross, Many-body interferometry of a Rydberg-dressed spin lattice, *Nat. Phys.* **12**, 1095 (2016).
- [15] J. Zeiher, J. Y. Choi, A. Rubio-Abadal, T. Pohl, R. van Bijnen, I. Bloch, and C. Gross, Coherent Many-Body Spin Dynamics in a Long-Range Interacting Ising Chain, *Phys. Rev. X* **7**, 041063 (2017).
- [16] A. Omran, H. Levine, A. Keesling, G. Semeghini, T. T. Wang, S. Ebadi, H. Bernien, A. S. Zibrov, H. Pichler, S. Choi *et al.*, Generation and manipulation of schrödinger cat states in Rydberg atom arrays, *Science* **365**, 570 (2019).
- [17] V. Borish, O. Marković, J. A. Hines, S. V. Rajagopal, and M. Schleier-Smith, Transverse-Field Ising Dynamics in a Rydberg-Dressed Atomic Gas, *Phys. Rev. Lett.* **124**, 063601 (2020).
- [18] A. Browaeys and T. Lahaye, Many-body physics with individually controlled Rydberg atoms, *Nat. Phys.* **16**, 132 (2020).
- [19] L. Henriët, L. Beguin, A. Signoles, T. Lahaye, A. Browaeys, G.-O. Reymond, and C. Jurczak, Quantum computing with neutral atoms, *Quantum* **4**, 327 (2020).
- [20] H. Bernien, S. Schwartz, A. Keesling, H. Levine, A. Omran, H. Pichler, S. Choi, A. S. Zibrov, M. Endres, M. Greiner *et al.*, Probing many-body dynamics on a 51-atom quantum simulator, *Nature (London)* **551**, 579 (2017).
- [21] A. Keesling, A. Omran, H. Levine, H. Bernien, H. Pichler, S. Choi, R. Samajdar, S. Schwartz, P. Silvi, S. Sachdev *et al.*, Quantum kibble-zurek mechanism and critical dynamics on a programmable Rydberg simulator, *Nature (London)* **568**, 207 (2019).
- [22] S. Ebadi, T. T. Wang, H. Levine, A. Keesling, G. Semeghini, A. Omran, D. Bluvstein, R. Samajdar, H. Pichler, W. W. Ho *et al.*, Quantum phases of matter on a 256-atom programmable quantum simulator, *Nature (London)* **595**, 227 (2021).
- [23] P. Scholl, M. Schuler, H. J. Williams, A. A. Eberharter, D. Barredo, K.-N. Schymik, V. Lienhard, L.-P. Henry, T. C. Lang,

- T. Lahaye *et al.*, Quantum simulation of 2d antiferromagnets with hundreds of Rydberg atoms, *Nature (London)* **595**, 233 (2021).
- [24] D. Bluvstein, A. Omran, H. Levine, A. Keesling, G. Semeghini, S. Ebadi, T. T. Wang, A. A. Michailidis, N. Maskara, W. W. Ho *et al.*, Controlling quantum many-body dynamics in driven Rydberg atom arrays, *Science* **371**, 1355 (2021).
- [25] P. Scholl, H. J. Williams, G. Bornet, F. Wallner, D. Barredo, L. Henriët, A. Signoles, C. Hainaut, T. Franz, S. Geier *et al.*, Microwave engineering of programmable $x \times x$ Hamiltonians in arrays of Rydberg atoms, *PRX Quantum* **3**, 020303 (2022).
- [26] S. Ohler, M. Kiefer-Emmanouilidis, A. Browaeys, H. P. Büchler, and M. Fleischhauer, Self-generated quantum gauge fields in arrays of Rydberg atoms, *New J. Phys.* **24**, 023017 (2022).
- [27] R. Kaurbruegger, P. Silvi, C. Kokail, R. van Bijnen, A. M. Rey, J. Ye, A. M. Kaufman, and P. Zoller, Variational Spin-Squeezing Algorithms on Programmable Quantum Sensors, *Phys. Rev. Lett.* **123**, 260505 (2019).
- [28] J. Van Damme, X. Zheng, M. Saffman, M. G. Vavilov, and S. Kolkowitz, Impacts of random filling on spin squeezing via Rydberg dressing in optical clocks, *Phys. Rev. A* **103**, 023106 (2021).
- [29] N. Schine, A. W. Young, W. J. Eckner, M. J. Martin, and A. M. Kaufman, Long-lived bell states in an array of optical clock qubits, *Nat. Phys.* **18**, 1067 (2022).
- [30] D. Jaksch, J. I. Cirac, P. Zoller, S. L. Rolston, R. Côté, and M. D. Lukin, Fast Quantum Gates for Neutral Atoms, *Phys. Rev. Lett.* **85**, 2208 (2000).
- [31] I. I. Beterov, M. Saffman, E. A. Yakshina, V. P. Zhukov, D. B. Tretyakov, V. M. Entin, I. I. Ryabtsev, C. W. Mansell, C. McCormick, S. Bergamini, and M. P. Fedoruk, Quantum gates in mesoscopic atomic ensembles based on adiabatic passage and Rydberg blockade, *Phys. Rev. A* **88**, 010303(R) (2013).
- [32] T. Keating, R. L. Cook, A. M. Hankin, Y.-Y. Jau, G. W. Biedermann, and I. H. Deutsch, Robust quantum logic in neutral atoms via adiabatic Rydberg dressing, *Phys. Rev. A* **91**, 012337 (2015).
- [33] I. I. Beterov, M. Saffman, E. A. Yakshina, D. B. Tretyakov, V. M. Entin, S. Bergamini, E. A. Kuznetsova, and I. I. Ryabtsev, Two-qubit gates using adiabatic passage of the stark-tuned forster resonances in Rydberg atoms, *Phys. Rev. A* **94**, 062307 (2016).
- [34] I. I. Beterov, G. N. Hamzina, E. A. Yakshina, D. B. Tretyakov, V. M. Entin, and I. I. Ryabtsev, Adiabatic passage of radio-frequency-assisted forster resonances in Rydberg atoms for two-qubit gates and the generation of bell states, *Phys. Rev. A* **97**, 032701 (2018).
- [35] M. Saffman, I. I. Beterov, A. Dalal, E. J. Páez, and B. C. Sanders, Symmetric Rydberg controlled-z gates with adiabatic pulses, *Phys. Rev. A* **101**, 062309 (2020).
- [36] I. I. Beterov, D. Tretyakov, V. Entin, E. Yakshina, I. Ryabtsev, M. Saffman, and S. Bergamini, Application of adiabatic passage in Rydberg atomic ensembles for quantum information processing, *J. Phys. B: At., Mol. Opt. Phys.* **53**, 182001 (2020).
- [37] A. Mitra, M. J. Martin, G. W. Biedermann, A. M. Marino, P. M. Poggi, and I. H. Deutsch, Robust mølmer-sørensen gate for neutral atoms using rapid adiabatic Rydberg dressing, *Phys. Rev. A* **101**, 030301(R) (2020).
- [38] X. L. Zhang, L. Isenhower, A. T. Gill, T. G. Walker, and M. Saffman, Deterministic entanglement of two neutral atoms via Rydberg blockade, *Phys. Rev. A* **82**, 030306(R) (2010).
- [39] T. Wilk, A. Gaëtan, C. Evellin, J. Wolters, Y. Miroshnychenko, P. Grangier, and A. Browaeys, Entanglement of Two Individual Neutral Atoms Using Rydberg Blockade, *Phys. Rev. Lett.* **104**, 010502 (2010).
- [40] H. Levine, A. Keesling, A. Omran, H. Bernien, S. Schwartz, A. S. Zibrov, M. Endres, M. Greiner, V. Vuletić, and M. D. Lukin, High-Fidelity Control and Entanglement of Rydberg-Atom Qubits, *Phys. Rev. Lett.* **121**, 123603 (2018).
- [41] T. M. Graham, M. Kwon, B. Grinkemeyer, Z. Marra, X. Jiang, M. T. Lichtman, Y. Sun, M. Ebert, and M. Saffman, Rydberg Mediated Entanglement in a Two-Dimensional Neutral Atom Qubit Array, *Phys. Rev. Lett.* **123**, 230501 (2019).
- [42] H. Jo, Y. Song, M. Kim, and J. Ahn, Rydberg Atom Entanglements in the Weak Coupling Regime, *Phys. Rev. Lett.* **124**, 033603 (2020).
- [43] M. J. Martin, Y.-Y. Jau, J. Lee, A. Mitra, I. H. Deutsch, and G. W. Biedermann, A mølmer-sørensen gate with Rydberg-dressed atoms, *arXiv:2111.14677*.
- [44] I. S. Madjarov, A. Cooper, A. L. Shaw, J. P. Covey, V. Schkolnik, T. H. Yoon, J. R. Williams, and M. Endres, An Atomic-Array Optical Clock With Single-Atom Readout, *Phys. Rev. X* **9**, 041052 (2019).
- [45] S. Ma, A. P. Burgers, G. Liu, J. Wilson, B. Zhang, and J. D. Thompson, Universal Gate Operations on Nuclear Spin Qubits in an Optical Tweezer Array of ^{171}Yb Atoms, *Phys. Rev. X* **12**, 021028 (2022).
- [46] J.-E. Johnson and S.-L. Rolston, Interactions between Rydberg-dressed atoms, *Phys. Rev. A* **82**, 033412 (2010).
- [47] Y.-Y. Jau, A. Hankin, T. Keating, I. Deutsch, and G. Biedermann, Entangling atomic spins with a Rydberg-dressed spin-flip blockade, *Nat. Phys.* **12**, 71 (2016).
- [48] X. L. Zhang, A. T. Gill, L. Isenhower, T. G. Walker, and M. Saffman, Fidelity of a Rydberg-blockade quantum gate from simulated quantum process tomography, *Phys. Rev. A* **85**, 042310(R) (2012).
- [49] S. de Léséleuc, D. Barredo, V. Lienhard, A. Browaeys, and T. Lahaye, Analysis of imperfections in the coherent optical excitation of single atoms to Rydberg states, *Phys. Rev. A* **97**, 053803 (2018).
- [50] T. Keating, K. Goyal, Y.-Y. Jau, G. W. Biedermann, A. J. Landahl, and I. H. Deutsch, Adiabatic quantum computation with Rydberg-dressed atoms, *Phys. Rev. A* **87**, 052314 (2013).
- [51] J. H. Wesenberg, K. Mølmer, L. Rippe, and S. Kröll, Scalable designs for quantum computing with rare-earth-ion-doped crystals, *Phys. Rev. A* **75**, 012304 (2007).
- [52] H. Saßmannshausen and J. Deiglmayr, Observation of Rydberg-Atom Macrodimers: Micrometer-Sized Diatomic Molecules, *Phys. Rev. Lett.* **117**, 083401 (2016).
- [53] S. Hollerith, K. Srakaew, D. Wei, A. Rubio-Abadal, D. Adler, P. Weckesser, A. Kruckenhauser, V. Walther, R. van Bijnen, J. Rui, C. Gross, I. Bloch, and J. Zeiher, Realizing Distance-Selective Interactions in a Rydberg-Dressed Atom Array, *Phys. Rev. Lett.* **128**, 113602 (2022).

- [54] F. Robicheaux, T.-M. Graham, and M. Saffman, Photon-recoil and laser-focusing limits to Rydberg gate fidelity, *Phys. Rev. A* **103**, 022424 (2021).
- [55] J. Lee, M. J. Martin, Y.-Y. Jau, T. Keating, I. H. Deutsch, and G. W. Biedermann, Demonstration of the jaynes-cummings ladder with Rydberg-dressed atoms, *Phys. Rev. A* **95**, 041801(R) (2017).
- [56] M. A. Nielsen, C. M. Dawson, J. L. Dodd, A. Gilchrist, D. Mortimer, T. J. Osborne, M. J. Bremner, A. W. Harrow, and A. Hines, Quantum dynamics as a physical resource, *Phys. Rev. A* **67**, 052301 (2003).
- [57] J. Zhang, J. Vala, S. Sastry, and K. B. Whaley, Geometric theory of nonlocal two-qubit operations, *Phys. Rev. A* **67**, 042313 (2003).